ChemComm

COMMUNICATION

View Article Online
View Journal | View Issue

Cite this: *Chem. Commun.*, 2017, 53, 2479

Received 22nd November 2016,
Accepted 31st January 2017

DOI: 10.1039/c6cc09310h

rsc.li/chemcomm

Electrical bistability in a metal–organic framework modulated by reversible crystalline-to-amorphous transformations†

Jing-Wei Xiu,[a] Guan-E Wang,[a] Ming-Shui Yao,[a] Chun-Chuen Yang,[b] Chia-Her Lin[b] and Gang Xu*[a]

Electrically bistable materials have important applications in memory, displays, switches, sensors, and quantum computation. This communication reports a metal–organic framework (MOF) material as a new type of electrically bistable material. Taking advantage of the flexible structure of MOF materials, the electrically bistable states of the MOF were reversibly modulated between its crystalline and amorphous phases. Interestingly, the material's amorphous phase exhibited anomalously higher conductivity than the crystalline phase. Our results illustrated a convenient method to develop electrically bistable materials from MOFs.

Metal organic frameworks (MOFs) are crystalline porous materials that are constructed by assembling metal centers and organic ligands *via* coordination bonding.[1] Their highly regular pores, large surface areas, functional building blocks, and variable and designable crystal structures make them versatile in gas separation and storage, catalysis, luminescence, and ionic and electronic conduction.[2] MOFs are inherently inclined to display crystal-to-crystal or crystal-to-amorphous transformations under various external stimuli because of their relative weak coordination bonds, large amplitude displacement of the organic linker at the empty pore, and small enthalpic difference between different structures.[3,4] Interestingly, the physical properties of MOF materials are modulated along with their structural transformations.[5,6] Moreover, if their structures before and after transformation are stable and the transformation is reversible, materials with intriguing bistable physical properties can be achieved. This kind of material has important applications in memory, displays, switches, sensing, and quantum computation.[7] Based on structure transformation, the reversible switches of gas absorption, fluorescence, magnetism, and catalysts in MOFs have emerged, whereas the appealing electrical properties of MOFs have not yet been reported to show their reversible switching behavior.[8]

This communication presents the electrical bistability of a MOF material modulated by reversible crystalline-to-amorphous transformation for the first time. The crystalline phase **1** and amorphous phase **2** of $Cu[Cu(pdt)_2]$ (pdt = 2,3-pyrazinedithiolate) were both stable at room temperature and standard pressure. Phases **1** and **2** reversibly interconverted to each other by heating or soaking in acetonitrile, respectively. These phases presented interesting electrical bistability because of their structural differences. Interestingly, the conductivity of amorphous **2** was anomalously 130% higher than that of crystal **1**. The possible reasons for this unusual phenomenon were explored *via* detailed characterizations.

$Cu[Cu(pdt)_2]$ was previously synthesized *via* the reaction of $Na[Cu^{III}(pdt)_2]\cdot 2H_2O$ and CuI in an acetonitrile solution (for details, see the ESI†).[9] In the crystal structure of **1**, the N atoms in $[Cu(pdt)]^-$ ligands coordinated with Cu^+ ions to form one-dimensional channels with an open-window size of ~0.68 nm along the *c*-axis (Fig. 1a). Cu^+ is widely known as an electron donor, whereas $[Cu(pdt)_2]^-$ acts as an electron acceptor.[10] The combination of this donor–acceptor pair in the framework made **1** electronically conductive. Compared with the complex and high-cost preparation processes for inorganic amorphous semiconductors, such as amorphous silicon and amorphous metal oxides, **1** could be easily prepared *via* a solution reaction and transformed into its amorphous phase **2** by heating at 120 °C for 2 h.[11] As shown in Fig. 1b, the as-synthesized **1** exhibited sharp X-ray diffraction peaks, indicating its good crystallinity. After the transformation from **1** to **2**, the diffraction peaks of the sample vanished completely, suggesting that **2** was amorphous. After soaking amorphous **2** in acetonitrile for 6 h, the sample showed sharp peaks again. The newly generated peaks displayed the exact same positions as those of **1**, demonstrating the recovery from **2** to **1**. The abovementioned processes could be repeated several times. Interestingly, the recovery from **2** to **1** was selectively triggered by acetonitrile rather than other solvents, such as ether, water, ethanol, methanol, acetone, ammonia water, benzonitrile, butyronitrile and valeronitrile (Fig. S1, ESI†). This selectivity may be induced by the strong interaction between the framework of $Cu[Cu(pdt)_2]$ and acetonitrile. We performed

[a] *State Key Laboratory of Structural Chemistry, Fujian Institute of Research on the Structure of Matter, Chinese Academy of Sciences, Fuzhou, Fujian, P. R. China. E-mail: gxu@fjirsm.ac.cn*
[b] *Chung-yuan Christian University, Taoyuan, Taiwan*

† Electronic supplementary information (ESI) available. See DOI: 10.1039/c6cc09310h

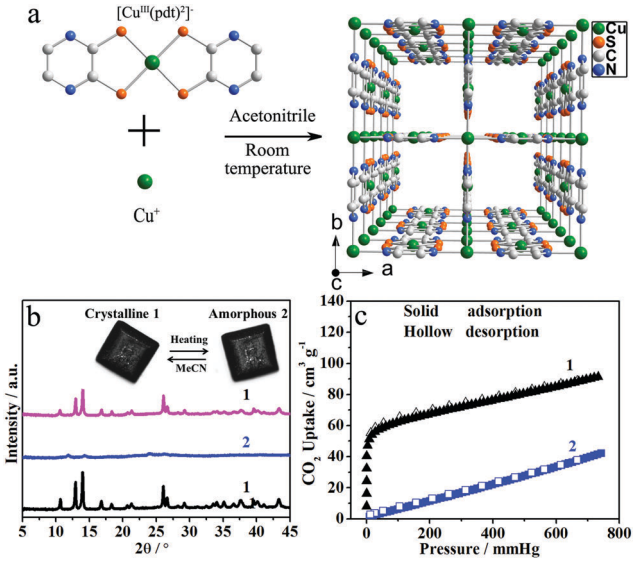

Fig. 1 (a) Crystal structure of Cu[Cu(pdt)$_2$]. Hydrogen atoms have been omitted for clarity. (b) PXRD patterns for the as-synthesized **1** (black), **2** (blue) and **1** (purple) obtained by soaking **2** in MeCN (inset: photographs of the bulk of single-crystal **1** and amorphous **2**; the lateral size of the single crystal is ~50 μm). (c) Sorption isotherms of CO_2 at 195 K for **1** and **2**.

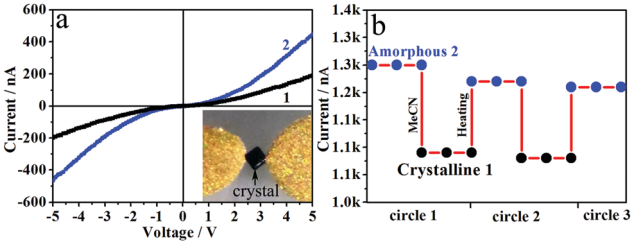

Fig. 2 (a) *I*–*V* curves of the same bulky sample of single crystal **1** and amorphous **2**; inset: single crystal (lateral size: ~50 μm) between the gold paste. (b) Reversible switches of the electrical conductivity of **1** and **2**.

multi-cycle acetonitrile sorption experiments to demonstrate this hypothesis (Fig. S2, ESI†). The sample was activated at 40 °C under high vacuum for 12 h. Then continuous measurements were conducted for the next 2 cycles without activation. For the fourth cycle, the sample was activated again with the same activation process as that for the first cycle. For the first cycle, the adsorption amount of acetonitrile reached as high as 0.09 g g^{-1} (P/P_0 = 1). However, it decreased significantly and remained stable at 0.05 g g^{-1} (P/P_0 = 1) for the second and third cycles. This phenomenon reveals the relative strong interaction between acetonitrile and the framework. However, this interaction can be eliminated by the activation process, which is demonstrated by the fact that the adsorption amount in the fourth cycle recovered to 0.09 g g^{-1} again. **1** and **2** had the same sizes and shapes during the structural transformation (the inset of Fig. 1b). **2** also slowly recovered to **1** in acetonitrile vapor. These observations revealed that the structural transformations between **1** and **2** were not a dissolution–recrystallization process.

The above-mentioned transformation processes could also be demonstrated using gas sorption measurements (Fig. 1c). The CO_2 sorption curves of **1** showed a microporous feature, which sharply adsorbed CO_2 at a very low relative pressure at 195 K. After heating at 120 °C *in situ* to form **2**, the sample showed a dramatic decrease in the adsorption of CO_2. This observation clearly indicated the collapse of the regular microporous framework of **1**.

The electrical properties of the single crystal of **1** and its derived bulky amorphous **2** were measured using a two-probe method (Fig. 2a). The opposite corners of the single crystal were painted with gold paste as electrodes. At room temperature, **1** and **2** have a current of 197 and 466 nA at 5 V, respectively. **2** exhibited a semiconducting behavior as shown in Fig. S3 and S4 (ESI†). Normally, for most semiconductors, such as In_2Se_3, SbN_2, and GeTe, the transformation from their crystalline to amorphous phase would induce a significant decrease of their conductivities (2–6 orders of magnitude) due to the absence of long-range ordered structures.[12] Surprisingly, the conductivity of amorphous **2** was 130% higher than that of crystalline **1**. This unexpected enhancement was carefully confirmed by more than five samples to exclude experimental errors. Notably, the conductivity of **1** in an acetonitrile atmosphere was higher than that in air (Fig. S5, ESI†), indicating that the conductivity of **1** is positively related to the amount of acetonitrile molecules inside its pore. This observation suggested the guest molecules inside **1** were not responsible for the lower conductivity of **1** compared to that of **2**.

The reversible switches between the electrical bistable states of Cu[Cu(pdt)$_2$] were demonstrated by an *in situ* study on the setups made by dip coating the crystallites of **1** in acetonitrile on ITO interdigital electrodes, because the gold paste for single crystal measurements is not stable in acetonitrile. Subsequently, the setup was maintained at 120 °C to remove acetonitrile and transformed **1** to **2**. As shown in Fig. 2b, the high and low conductive states of Cu[Cu(pdt)$_2$] were reproducibly switched by heating and immersing into acetonitrile, respectively. These processes could be repeated for several cycles with minimal signal fatigue. However, the change in conductivity between **1** and **2** in this case was only 14%, which was less than that of bulk samples. The reason for this smaller conductivity variation was attributed to the grain boundary among MOF particles.

To further analyze the unusual phenomenon that amorphous **2** has higher conductivity than **1**, both samples were fully characterized. Thermal gravimetric analysis data (Fig. S6, ESI†) showed that **1** gradually lost its lattice solvents in its pore when temperature was increased from 30 to 160 °C. After that, weight loss was not observed at temperature levels of up to 250 °C. The temperature for the transformation from **1** to **2** was 120 °C, which was far lower than the decomposition temperature of 250 °C. The reversible transformation between the crystalline and amorphous phases revealed that the frameworks of **1** and **2** had the same chemical compositions. The X-ray photoelectron spectroscopy (XPS) spectra of Na[Cu(pdt)$_2$]·2H$_2$O were compared with those of **1** and **2** to analyze the oxidation states of coppers (Fig. 3a). Two kinds of coppers were found in the structure of **1** with a mole ratio of 1 : 1. Cu^+ originated from the CuI reagent, while Cu^{3+} came from the reagent Na[Cu^{III}(pdt)$_2$]·2H$_2$O. The absence of satellite peaks of Cu $2p_{3/2}$ between 940 and 945 eV indicated the absence of Cu^{2+}.[13,14]

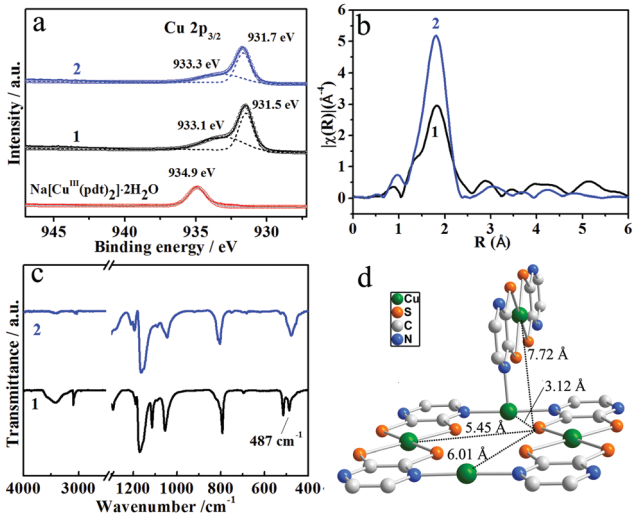

Fig. 3 (a) XPS spectra of **1**, **2**, and $Na[Cu(pdt)_2]\cdot 2H_2O$, showing the raw data, simulated spectra, and deconvoluted spectra as solid lines, circle lines, and dashed lines, respectively. (b) Radius distribution functions (RDFs) of the Fourier-transformed Cu K-edge EXAFS spectra. (c) FTIR spectra of **1** and **2**. (d) The distances of adjacent Cu and S atoms in **1**.

Compared with the spectrum of $Na[Cu^{III}(pdt)_2]\cdot 2H_2O$, the peak at 931.5 eV in **1** was assigned to Cu^+ because this peak was newly generated after the reaction of Cu^+ and $[Cu^{III}(pdt)_2]^-$. **1** and **2** showed similar Cu $2p_{3/2}$ peaks, indicating that they had the same ratio of Cu^+ and Cu^{3+}. These results demonstrated that both **1** and **2** had the same molecular formula of $Cu^I[Cu^{III}(pdt)_2]$. Therefore, the different conductivities between **1** and **2** originated from their structural rearrangement rather than their components or oxidation states.

In general, the coordination bonds between metals and ligands are relatively weaker compared with the covalent bonds in the rigid ligands.[4] The reagent $Na[Cu(pdt)_2]\cdot 2H_2O$ maintained its good crystallinity after treatment at 180 °C (Fig. S7, ESI†), indicating that the Cu–S bonds in $[Cu(pdt)_2]^-$ were stable at a temperature below 180 °C, which was 60 °C higher than the temperature for the structural transformation from **1** to **2**. Compared with monodentate Cu–N coordination, the polydentate coordination mode of Cu–S bonds and the five-membered rings formed by Cu–S coordination were superior in stability (Fig. 1). Moreover, the bond energy calculation revealed that the energy of the Cu–S bond was −447 kcal mol^{-1}, which was much more exothermic than that of the Cu–N bond (−28 kcal mol^{-1}) (see the ESI†). Therefore, the Cu–S bond was more stable than the Cu–N bond in **1**. From the analyses above, the transformation is more likely to start from the rearrangement of Cu–N bonds, which are thought to be the weakest parts in the framework structure of **1**.[15] The abovementioned results were further confirmed by Raman spectra of **1** and **2** (Fig. S8, ESI†). The peak at 334 cm^{-1} in **1** was assigned to Cu–N stretching, whereas the peaks at 192 and 160 cm^{-1} were assigned to the N–Cu–N modes.[16] After the transformation from **1** to **2**, the peak at 192 cm^{-1} shifted to 208 cm^{-1} with decreased intensity, and a new peak appeared at 244 cm^{-1}. These results indicated that N–Cu–N was significantly distorted.

Besides the distortion of N–Cu–N bonds, our Fourier-transformed Cu K-edge extended X-ray absorption fine structure (EXAFS) measurements revealed that new bonds were generated in the transformation from **1** to **2**. As illustrated in Fig. 3b, both the spectra of **1** and **2** showed a strong peak at 1.7 Å, which corresponded to Cu–S and Cu–N in the first copper coordination shell according to FEFF simulation based on the single-crystal XRD data. The enhanced intensity of this peak in **2** compared with that in **1** suggested that the coordination number of Cu increased after structural transformation.[17] Fourier transform infrared spectroscopy (FTIR) measurements (Fig. 3c and Fig. S9, ESI†) were conducted to reveal further details about the increment in the Cu coordination number. The vibrational peak at 487 cm^{-1} in the IR spectrum of **1** was assigned to Cu–S stretching vibration.[18] This peak was significantly strengthened, which may suggest an increment in Cu–S bonds. The newly generated Cu–S bonds originated from the connections of Cu and S atoms in the adjacent ligands during structural transformation. The broadening of this peak might be due to the appearance of a new type of coordination geometry of Cu, for example, from an all equal square-planner type to a non-equal type. In the structure of **1** (Fig. 3d), the closest distance between the unconnected Cu and S was as short as 3.12 Å, which was even shorter than the sum of their Van der Waals radius (3.2 Å) and most likely to generate a new Cu–S bond. Other adjacent Cu and S atoms may also connect if they were close enough during structural transformation.

The reversible transformation of the frameworks was closely related to the removal and adsorption of acetonitrile. Although the patterns of PXRD changed significantly, **1** and **2** had similar chemical bonds according to their IR, XPS and EXAFS. So, the structural change between **1** and **2** might not involve a significant displacement of the Cu-ions and the linker but possibly *via* a rotated/twisted coordination sphere of copper. During the structural transformation from **1** to **2**, the N–Cu–N bonds were distorted, and the total ligancy of Cu increased because of the generation of new Cu–S bonds. Importantly, the electron donor–acceptor pair for conduction was conserved during structural transformation, and the new Cu–S bonds provided additional pathways for electron transportation. These results are an important basis for the unusual enhanced conductivity of **2** compared with **1**.[5,13]

Therefore, this communication reports an interesting electrical bistability of an MOF material, $Cu[Cu(pdt)_2]$, which was reversibly modulated by its crystalline and amorphous transformations. In contrast to traditional semiconductors, the amorphous phase of $Cu[Cu(pdt)_2]$ showed anomalously higher conductivity than the crystalline phase, which is extremely desirable for the application of amorphous semiconductors. Detailed characterizations revealed that this unusual electrical phenomenon was attributed to the conservation of functional groups in the structure and the generation of new Cu–S bonds when the crystal state changed to the amorphous state. Given that MOFs have well established structural and compositional tenability as well as their structures can response to various external stimuli, our work may open the avenue to design and prepare electrically bistable materials from MOFs for applications in memories, displays, and switches.

This work was supported by NSFC (51402293), Strategic Priority Research Program, CAS (XDB20000000), NSF of Fujian for Distinguished Young Scholars (2016J06006), Key project of CAS (QYZDB-SSW-SLH023), and Fund for Returned Overseas Chinese Scholars sponsored by MHRSS of Fujian. We also thank Prof. M. Dong for the valuable discussions on EXAFS and Prof. C. S. Li and Dr J. S. Song for the calculations of bonding energy.

Notes and references

1 P. Silva, S. M. F. Vilela, J. P. C. Tome and F. A. Almeida Paz, *Chem. Soc. Rev.*, 2015, **44**, 6774.
2 P. Ramaswamy, N. E. Wong, B. S. Gelfand and G. K. H. Shimizu, *J. Am. Chem. Soc.*, 2015, **137**, 7640; F. Sun, Z. Yin, Q. Q. Wang, D. Sun, M. H. Zeng and M. Kurmoo, *Angew. Chem., Int. Ed.*, 2013, **52**, 4538; Y. Ye, L. Zhang, Q. Peng, G. E. Wang, Y. Shen, Z. Li, L. Wang, X. Ma, Q. H. Chen, Z. Zhang and S. C. Xiang, *J. Am. Chem. Soc.*, 2015, **137**, 913; S. S. Han, W. Q. Deng and W. A. Goddard, *Angew. Chem., Int. Ed.*, 2007, **46**, 6289; K. K. Tanabe and S. M. Cohen, *Angew. Chem., Int. Ed.*, 2009, **48**, 7424; S. S. Nagarkar, B. Joarder, A. K. Chaudhari, S. Mukherjee and S. K. Ghosh, *Angew. Chem., Int. Ed.*, 2013, **52**, 2881; M. G. Campbell, D. Sheberla, S. F. Liu, T. M. Swager and M. Dinca, *Angew. Chem., Int. Ed.*, 2015, **54**, 4349; G. Xu, K. Otsubo, T. Yamada, S. Sakaida and H. Kitagawa, *J. Am. Chem. Soc.*, 2013, **135**, 7438.
3 M. Higuchi, K. Nakamura, S. Horike, Y. Hijikata, N. Yanai, T. Fukushima, J. Kim, K. Kato, M. Takata, D. Watanabe, S. Oshima and S. Kitagawa, *Angew. Chem., Int. Ed.*, 2012, **51**, 8369; A. Schneemann, V. Bon, I. Schwedler, I. Senkovska, S. Kaskel and R. A. Fischer, *Chem. Soc. Rev.*, 2014, **43**, 6062.
4 A. B. Cairns and A. L. Goodwin, *Chem. Soc. Rev.*, 2013, **42**, 4881.
5 T. D. Bennett, P. J. Saines, D. A. Keen, J. C. Tan and A. K. Cheetham, *Chem. – Eur. J.*, 2013, **19**, 7049.
6 T. D. Bennett and A. K. Cheetham, *Acc. Chem. Res.*, 2014, **47**, 1555.
7 I. Friedrich, V. Weidenhof, W. Njoroge, P. Franz and M. Wuttig, *J. Appl. Phys.*, 2000, **87**, 4130; S. Raoux, W. Wełnic and D. Ielmini, *Chem. Rev.*, 2010, **110**, 240; J. G. Champlain, L. B. Ruppalt, A. C. Guyette, N. El-Hinnawy, P. Borodulin, E. Jones, R. M. Young and D. Nichols, *J. Appl. Phys.*, 2016, **119**, 244501.
8 S. B. Choi, H. Furukawa, H. J. Nam, D. Y. Jung, Y. H. Jhon, A. Walton, D. Book, M. O'Keeffe, O. M. Yaghi and J. Kim, *Angew. Chem., Int. Ed.*, 2012, **51**, 8791; X. Yang and D. Yan, *Chem. Sci.*, 2016, **7**, 4519; S. Yuan, L. Zou, H. Li, Y. P. Chen, J. Qin, Q. Zhang, W. Lu, M. B. Hall and H.-C. Zhou, *Angew. Chem., Int. Ed.*, 2016, **55**, 10776; S. Sakaida, K. Otsubo, O. Sakata, C. Song, A. Fujiwara, M. Takata and H. Kitagawa, *Nat. Chem.*, 2016, **8**, 377; L. Cañadillas-Delgado, O. Fabelo, J. A. Rodríguez-Velamazán, M. H. Lemée-Cailleau, S. A. Mason, E. Pardo, F. Lloret, J. P. Zhao, X. H. Bu, V. Simonet, C. V. Colin and J. Rodríguez-Carvajal, *J. Am. Chem. Soc.*, 2012, **134**, 19772.
9 S. Takaishi, M. Hosoda, T. Kajiwara, H. Miyasaka, M. Yamashita, Y. Nakanishi, Y. Kitagawa, K. Yamaguchi, A. Kobayashi and H. Kitagawa, *Inorg. Chem.*, 2009, **48**, 9048.
10 X. Ribas, J. C. Dias, J. Morgado, K. Wurst, E. Molins, E. Ruiz, M. Almeida, J. Veciana and C. Rovira, *Chem. – Eur. J.*, 2004, **10**, 1691.
11 E. Fortunato, P. Barquinha and R. Martins, *Adv. Mater.*, 2012, **24**, 2945; G. Wang, Y. Chen, X. Shen, J. Li, R. Wang, Y. Lu, S. Dai, T. Xu and Q. Nie, *ACS Appl. Mater. Interfaces*, 2014, **6**, 8488; P. Barquinha, L. Pereira, G. Gonçalves, R. Martins and E. Fortunato, *J. Electrochem. Soc.*, 2009, **156**, H161.
12 C. S. Hwang, *Adv. Electron. Mater.*, 2015, **1**, 1400056.
13 S. Tominaka, H. Hamoudi, T. Suga, T. D. Bennett, A. B. Cairns and A. K. Cheetham, *Chem. Sci.*, 2015, **6**, 1465.
14 H. Rupp and U. Weser, *Biochim. Biophys. Acta*, 1976, **446**, 151.
15 T. D. Bennett, A. L. Goodwin, M. T. Dove, D. A. Keen, M. G. Tucker, E. R. Barney, A. K. Soper, E. G. Bithell, J. C. Tan and A. K. Cheetham, *Phys. Rev. Lett.*, 2010, **104**, 115503.
16 S. Brown, J. Cao, J. L. Musfeldt, M. M. Conner, A. C. McConnell, H. I. Southerland, J. L. Manson, J. A. Schlueter, M. D. Phillips, M. M. Turnbull and C. P. Landee, *Inorg. Chem.*, 2007, **46**, 8577.
17 S. Horike, W. Chen, T. Itakura, M. Inukai, D. Umeyama, H. Asakura and S. Kitagawa, *Chem. Commun.*, 2014, **50**, 10241.
18 M. E. Helton, P. Chen, P. P. Paul, Z. Tyeklár, R. D. Sommer, L. N. Zakharov, A. L. Rheingold, E. I. Solomon and K. D. Karlin, *J. Am. Chem. Soc.*, 2003, **125**, 1160.

